Bioinspired Hydrogel Interferometer for Adaptive Coloration and Chemical Sensing

Meng Qin, Mo Sun, Ruobing Bai, Yiqi Mao, Xiaoshi Qian, Dipika Sikka, Yuan Zhao, Hang Jerry Qi, Zhigang Suo, and Ximin He*

Living organisms ubiquitously display colors that adapt to environmental changes, relying on the soft layer of cells or proteins. Adoption of soft materials into an artificial adaptive color system has promoted the development of material systems for environmental and health monitoring, anti-counterfeiting, and stealth technologies. Here, a hydrogel interferometer based on a single hydrogel thin film covalently bonded to a reflective substrate is reported as a simple and universal adaptive color platform. Similar to the cell or protein soft layer of color-changing animals, the soft hydrogel layer rapidly changes its thickness in response to external stimuli, resulting in instant color change. Such interference colors provide a visual and quantifiable means of revealing rich environmental metrics. Computational model is established and captures the key features of hydrogel stimuli-responsive swelling, which elucidates the mechanism and design principle for the broad-based platform. The single material–based platform has advantages of remarkable color uniformity, fast response, high robustness, and facile fabrication. Its versatility is demonstrated by diverse applications: a volatile-vapor sensor with highly accurate quantitative detection, a colorimetric sensor array for multianalyte recognition, breath-controlled information encryption, and a colorimetric humidity indicator. Portable and easy-to-use sensing systems are demonstrated with smartphone-based colorimetric analysis.

Many animals can change their colors for acclimatization, camouflage, and communication, by tuning the volume or thickness of their cell or protein soft layer. For example, cephalopods (squid, cuttlefish, octopus) rapidly adapt their skin colors to the environment by expanding or contracting the chromatophores. Upon external stimuli, cephalopods would contract or relax radial muscles that are attached to the chromatophores, leading to increased or decreased area of the pigmented sac of a chromatophore.[1,2] Among the cephalopods, some squids (e.g., *Euprymna scolopes*) possess iridophores that lie underneath the chromatophores. The iridophores can produce iridescent colors, which are generated from the light reflection of reflectin platelet stacks in iridophores and can be tuned with the thickness change of the platelets.[3,4] Besides these soft-bodied animals, longhorn beetle *Tmesisternus isabellae* (*T. isabellae*) changes the color of its elytron from green to red when the ambient humidity increases. The elytron contains photonic structures of alternative layers, of which one is a melanoprotein layer, and the other is a mixed layer of melanoprotein and air voids. When the ambient humidity increases, melanoprotein would absorb water molecules and swell, inducing the color change of elytron.[5,6] These typical examples reveal that such adaptive colors are realized by the change in volume or thickness of the cell or protein soft layer in response to environmental cues such as change in humidity, light, temperature, and concentrations of specific molecules. Inspired by this strategy of nature, applying soft materials to advance artificial adaptive coloring could promote the development of various areas such as sensing, displays, optical filters, anti-counterfeiting, and stealth technologies.

Hydrogels are a class of promising soft materials that can change their volume by severalfold in response to a small alteration of environmental cues.[7,8] The polymer network of hydrogels can be readily functionalized to respond to cues like temperature, pH, and a wide range of specific molecules.[9–13] Furthermore, most hydrogels are transparent and stretchable, as well as low cost and environmentally friendly.[14,15] Hydrogels have been used as stimuli-responsive components in structural color systems commonly in the form of photonic crystals.[16–23] As photonic crystals rely on highly ordered structures and periodically arranged refractive indices, this requires careful coassembling of multiple materials and micro-/nanobuilding blocks to produce uniform color in large scale, limiting their rapid and convenient fabrication.[24] In addition, the multilayer structures

Dr. M. Qin, Dr. M. Sun, Dr. X. Qian, D. Sikka, Dr. Y. Zhao, Prof. X. He
Department of Materials Science and Engineering
University of California, Los Angeles
Los Angeles, CA 90095, USA
E-mail: ximinhe@ucla.edu
R. Bai, Prof. Z. Suo
John A. Paulson School of Engineering and Applied Sciences
Kavli Institute for Bionano Science and Technology
Harvard University
Cambridge, MA 02138, USA
Dr. Y. Mao, Prof. H. J. Qi
The George Woodruff School of Mechanical Engineering
Georgia Institute of Technology
Atlanta, GA 30332, USA

The ORCID identification number(s) for the author(s) of this article can be found under https://doi.org/10.1002/adma.201800468.
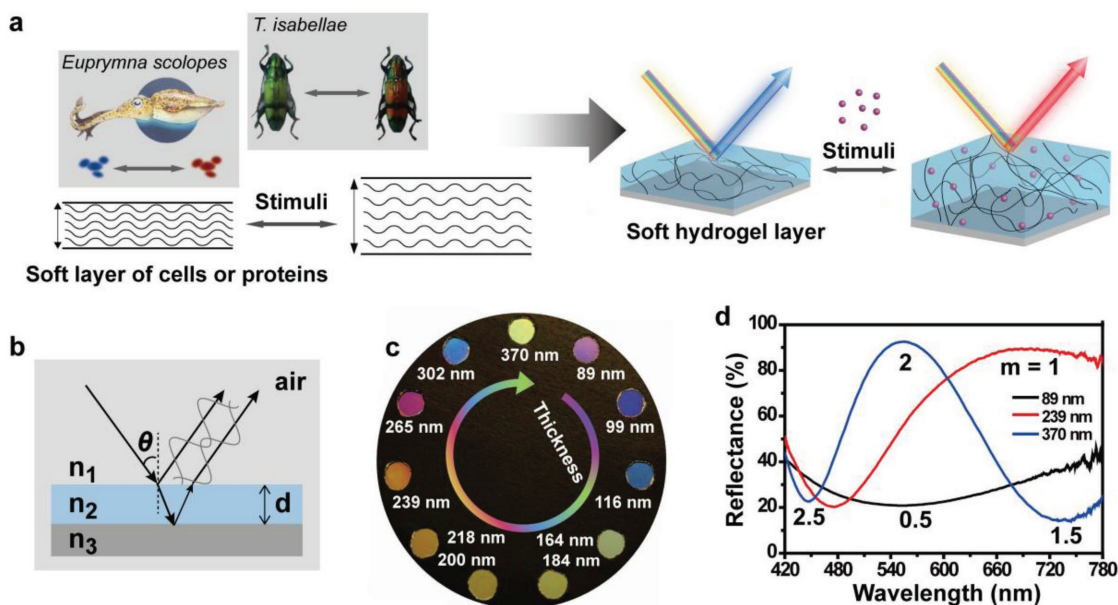
Figure 1. Color generation of the hydrogel interferometer. a) Animals change color by tuning the volume or thickness of cell or protein soft layer, inspiring the design of soft hydrogel layer–based adaptive color platform. The image of *T. isabellae* is reproduced from ref. [6] b) Schematic of interference of the two reflected light waves from the air–hydrogel and hydrogel–substrate interfaces. n_1, n_2, n_3 are the refractive indices of air, hydrogel, and silicon, respectively. d is the thickness of hydrogel. θ is the incident angle. c) Photograph of a color palette of hydrogel films with tunable thickness and d) the corresponding reflection spectra at an incident angle of 0°. The films show colors determined by reflection peaks ($m = 1, 2$) or complementary colors ($m = 0.5, 1.5, 2.5$) determined by reflection valleys.

prolong the time needed for swelling and hinder their applications for real-time monitoring.[25]

Here, we report an adaptive color system of a particularly simple design: a single layer of hydrogel on a reflective substrate. In contrast to the commonly used micro-/nanobuilding blocks, the hydrogel film is featureless and can be readily fabricated with excellent homogeneity, exhibiting uniform color. The colors arise from the interference of the light waves reflected from the air–hydrogel interface and the hydrogel–substrate interface. Similar to the cell or protein soft layer of color-changing animals, the soft hydrogel layer can rapidly change its thickness in response to external stimuli, resulting in instant color change (**Figure 1**a). The hydrogel film is covalently bonded to the substrate, with well-controlled thickness at 100 nm scale. The film is thin, enabling fast swelling. A computational model has been established to investigate both the ratio and the rate of the hydrogel-responsive swelling, which validated experimental results and elucidated the mechanism. This adaptive color platform provides a means of unveiling chemical signals by visual and quantifiable color change. Based on this hydrogel interferometer, we have demonstrated a volatile-vapor sensor, presenting highly accurate quantitative detection with response and recovery times to full equilibrium of 140 and 210 ms, respectively, much faster than the previously reported hydrogel-based volatile-vapor sensors (Table S1, Supporting Information).[26–28] By simply arranging the same sensors with different thicknesses into an array, we have further realized multianalyte recognition. Owing to the facile photopatterning of the photocurable hydrogel, we have also developed breath-controlled information encryption and humidity indicators. Furthermore, we have established smartphone-based colorimetric analysis to

make the hydrogel interferometer a portable and easy-to-use sensing system. This adaptive color system may advance real-time environment monitoring, point-of-care technology, and remote sensing data collection.

The hydrogel interferometer was prepared by a one-step method, with spin-coating deposition and in situ polymerization of hydrogel precursor solutions onto a reflective substrate. The whole procedure was completed within minutes. A silicon (Si) wafer modified to allow covalent bonding with the hydrogel was used as the substrate[29] (Figure S1, Supporting Information). The adaptive coloration of such a simple structure that comprises only one homogenous hydrogel layer on a reflective substrate is shown to obey a simple governing equation of thin-film interference physics as follows. The color is generated by interference of the two reflected light waves from the air–hydrogel and hydrogel–substrate interfaces (Figure 1b). The refractive indices of air, hydrogel, and silicon are $n_1 = 1$, $n_2 = 1.52$, and $n_3 = 3.8$, respectively. In the case of $n_1 < n_2 < n_3$, the condition for constructive interference is $2n_2 d\cos\theta = m\lambda$, and the condition for destructive interference is $2n_2 d\cos\theta = (m - 0.5)\lambda$, where d is the thickness of hydrogel, θ is the angle of incident wave, λ is the wavelength of interference light, and m is an integer.[30] At normal incidence ($\cos\theta = 1$), the color is mainly determined by the thickness of hydrogel film, where the thickness d is comparable to the wavelength of visible light. As shown in Figure 1c, with an increase in thickness from 89 to 370 nm, the hydrogel films show a broad color spectrum from violet to yellow-green. The colors correspond to the peaks (constructive interference) and valleys (destructive interference) in the reflection spectra (Figure 1d, see detailed discussion in Figure S3 in the Supporting Information). The reflected light

ADVANCED
SCIENCE NEWS
www.advancedsciencenews.com

ADVANCED
MATERIALS
www.advmat.de

interference–based color is confirmed by good agreement of the experimental values and the theoretical locations of constructive and destructive interference calculated from the equations (Figure S4, Supporting Information).

To investigate the response of the hydrogel interferometer, a poly(2-hydroxyethyl methacrylate-*co*-acrylic acid) (poly(HEMA-*co*-AAc)) hydrogel interferometer (Fourier transform infrared (FT-IR) spectra shown in Figure S5 in the Supporting Information) was prepared to act as a volatile-vapor sensor (ethanol as a model vapor). In the reference state, a poly(HEMA-*co*-AAc) film of a thickness of 233 nm at ambient condition exhibits an orange color, with the second-order destructive interference centered at 472 nm (Figure S6, Supporting Information). When exposed to ethanol vapor (saturated with nitrogen gas (N_2)), the hydrogel film swells and rapidly changes its color to blue, with a redshift of the valley from 472 to 577 nm and the occurrence of the second-order constructive interference centered at 441 nm. We carried out real-time monitoring of the reflectance centered at 472 nm (30 data points in the range of 472 ± 5 nm were used to avoid inaccuracy) to investigate the response and recovery of the hydrogel film between the reference state and the fully swollen state. As shown in **Figure 2**a, when the film is exposed to ethanol vapor, the reflectance at 472 nm increases instantly and then decreases immediately after the vapor is removed. The measured response and recovery time for saturated ethanol vapor are 140 and 210 ms, respectively. For diluted ethanol vapor (diluted by N_2 to 50% of the saturation pressure, Figure S7, Supporting Information), it still shows the similar fast response, indicating good ethanol sensitivity of the poly(HEMA-*co*-AAc) hydrogel. Compared with current state-of-the-art colorimetric ethanol vapor sensors, which typically exhibit response

time of several seconds and even longer recovery time, this hydrogel interferometer responds much faster.[31,32] Such sub-second response time is mainly attributed to two reasons: first, hydrogen bonding and the similarity of the solubility parameters of poly(HEMA-*co*-AAc) and ethanol result in strong affinity between the polymer network and the vapor, leading to rapid absorption and diffusion of ethanol vapor;[28,33,34] second, the sub-micrometer-scale thickness of the film enables ultrashort diffusion length and thus fast diffusion of analytes to achieve equilibrium of swelling, which also benefits the rapid desorption and leads to a short recovery time. In addition, the sensor shows great robustness, since the response–recovery cycles can be carried out repeatedly with highly consistent performance (Movie S1, Supporting Information).

The hydrogel interferometer was then applied to sense various concentrations of ethanol vapor with colorimetric analysis. The effective refractive index of hydrogel changes slightly upon the absorption of ethanol vapor, which is trivial compared with the thickness change of hydrogel and therefore makes negligible effect to interference (Figure S8, Supporting Information). Figure 2b shows the thickness change of a hydrogel film sensor (initial thickness of 224 nm) with increased concentration of ethanol vapor mixed by N_2, with P as the partial pressure of ethanol in the mixture, and P_0 the saturation pressure of ethanol (corresponding to a concentration of $\approx$163 $\mu g\ mL^{-1}$). The experimental data match well with the theoretical prediction obtained by simulation based on a hydrogel swelling model (see details in the Supporting Information).[35,36] With the increase of ethanol vapor concentration, the chemical potential of ethanol in the surrounding increases as well, leading to more ethanol diffusing into the hydrogel. As a result, in the relatively high ethanol vapor concentration range, the hydrogel film exhibits
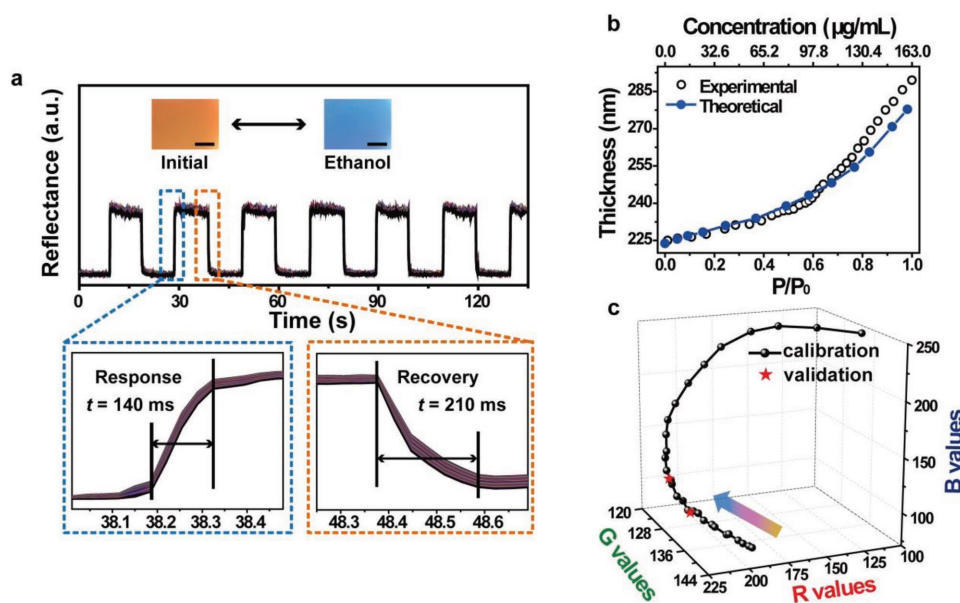

Figure 2. Ethanol vapor sensor based on poly(HEMA-*co*-AAc) hydrogel interferometer. a) Real-time monitoring of ethanol indicated by the reflectance change of the second-order destructive interference centered at 472 nm. The reflectance increases when the sensor is exposed to ethanol vapor (saturated with N_2) and decreases when ethanol vapor is removed. The insets show optical images of the film before and after ethanol response. The scale bar is 500 μm. b) Experimental and theoretical hydrogel film thickness as a function of the partial pressure of ethanol. c) Quantitative analysis of ethanol vapor concentration based on RGB values. Two analyte samples are used for validation. The arrow indicates increase in the partial pressure of ethanol.

more significant swelling, with faster thickness rise (can also be observed in the simulation results, Figure S18, Supporting Information). The detection limit of the sensor is 1.74 µg mL^{-1} for ethanol vapor, restricted by the resolution of the fiber optic spectrometer (1.5 nm), demonstrating remarkable sensing performance comparable to the reported sensors.[37,38] We then carried out a quantitative colorimetric analysis to detect the ethanol vapor by analyzing red, green, and blue (RGB) color channels. As shown in Figure 2c, with increased vapor concentration from 0 to P_0, corresponding to color change of the sensor from yellow to violet (Figure S9, Supporting Information), the R values increase first and then decrease; oppositely, the G values decrease first and then increase; the B values always increase. To investigate the accuracy of the quantitative detection, we divided the acquired data into two groups, one for constructing a calibration curve and the other to be used as unknown analyte samples for validation. By projecting the RGB space onto a 2D hyperplane score plot through principle component analysis, the unknown concentration can be determined by calculating the Euclidean distances between the validation point and its adjacent data (Figure S10, Supporting Information).[39] The estimated concentrations of the two analyte samples are 90.56 and 107.24 µg mL^{-1}, respectively. Compared with their actual concentrations as 90.64 and 108.74 µg mL^{-1}, the errors are 0.09% and 1.38%, respectively, indicating highly accurate estimation. Similar results were obtained by using a sensor with film thickness of 281 nm (Figure S11 and Table S2, Supporting Information).

By integration of the hydrogel interferometers into a sensor array, multianalyte recognition can be realized, with only one hydrogel material of different thicknesses. Generally, the construction of sensor arrays requires complex synthesis and massive screening of sensing molecules, or cooperation of multiple materials, making it a challenge for facile design with minimum materials.[40–43] **Figure 3**a shows a sensor array composed of poly(HEMA-*co*-AAc) of three different film thicknesses (234 nm for S1, 290 nm for S2, 362 nm for S3). After being exposed to volatile organic compounds (VOCs, i.e., acetic acid, acetone, ethanol, ethyl acetate, hexane, isopropanol (IPA), methanol, and tetrahydrofuran (THF), all saturated with N$_2$), the sensor array shows a distinct color pattern for each VOC, due to the different swelling behaviors of the hydrogel in different vapors (Figure S12 and Table S3, Supporting Information). A single sensor may not give enough colorimetric information to differentiate the VOCs. For example, S1 shows similar violet color after responding to acetone and IPA, but S2 and S3 differentiate the two compounds. Figure 3b shows RGB-based response patterns of the sensor array to the VOCs. Each VOC possesses a specific pattern, even for chemically similar analytes such as alcohols (methanol, ethanol, and IPA). The identification of VOCs was performed by linear discriminant analysis (LDA) on the acquired data (8 VOCs × 3 RGB values × 3 sensors × 3 trails) to evaluate the similarity between data clusters (Figure 3c). $F1$ and $F2$ are the first two functions that describe the greatest spatial separation of the data. As shown in the 2D LDA score plot, clusters of different VOCs are significantly separated, showing 98.3% correct classification through the first two functions, which suggests successful discrimination. This single response material–based sensor array has provided a facile and effective strategy to differentiate multiple compounds.

The sensing elements with different film thicknesses can be realized on a single hydrogel interferometer through on-demand patterning by spatially controlled polymerization. To demonstrate this, we designed a series of patterned devices based on the commonly used poly(acrylamide-*co*-acrylic acid) hydrogel. As shown in **Figure 4**a, after spin coating and short-time ultraviolet (UV) exposure of the precursor solution, partially polymerized film was formed. Subsequently, additional UV exposure on selected regions of the film was conducted with a photomask to enable spatially controlled polymerization. Under this procedure, a freshly made platform appeared a uniform color without observable patterns. After being exposed to moisture, the encoded image area was revealed. Hence, the patterned platform serves as an information encryption device. As shown in Figure 4b, the encrypted letters "UCLA"
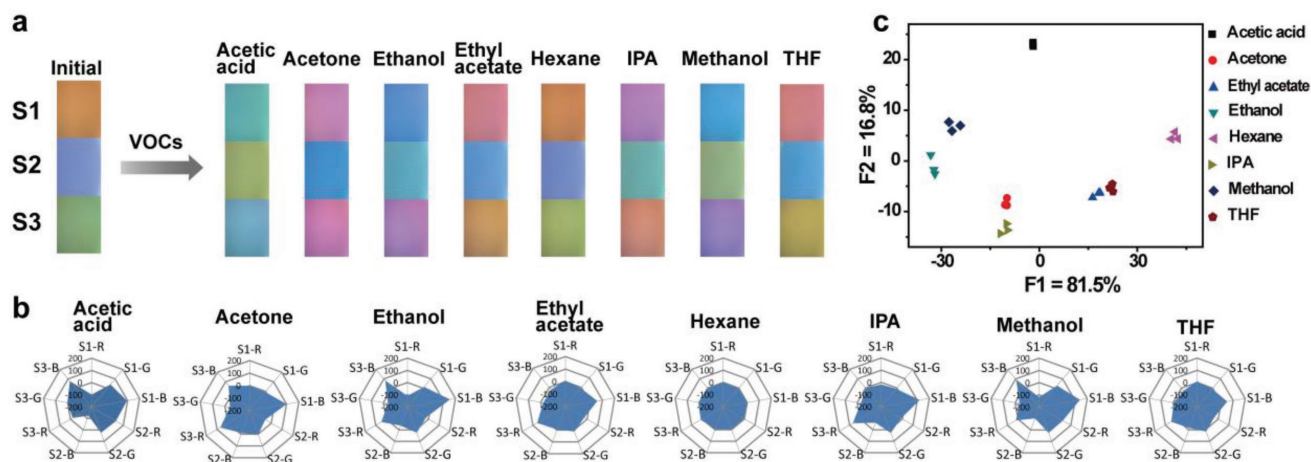

Figure 3. Pattern-based recognition of multiple VOCs with single hydrogel material–based sensor array. a) Colorimetric response of the sensor array to 8 VOCs. The three sensing elements are all based on poly(HEMA-*co*-AAc) hydrogel, with a thickness of 234 nm for S1, 290 nm for S2, 362 nm for S3, respectively. b) RGB value patterns of the sensor array to each VOC. c) The 2D score plot of LDA of 8 VOCs measured three times, showing significant separation of data clusters.
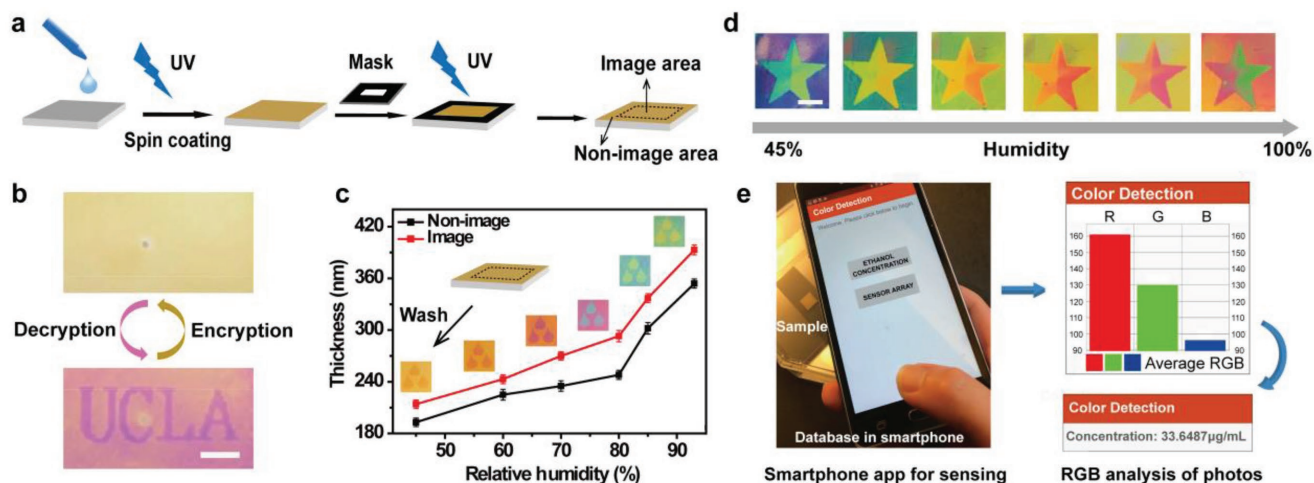
**ADVANCED
SCIENCE NEWS**
www.advancedsciencenews.com

**ADVANCED
MATERIALS**
www.advmat.de

Figure 4. Patterning of hydrogel interferometer and smartphone-based sensing. a) Schematic of the patterning process. On-demand patterning can be achieved through spatially controlled polymerization. b) An information encryption device. The decryption is triggered instantly by moisture, while the information is hidden immediately after removing moisture. The scale bar is 2 mm. c) Thickness changes of the image (water droplet pattern) and nonimage (surrounding) areas with increased relative humidity in the surrounding. The insets are the corresponding photographs of water droplet pattern at respective humidity. d) A humidity indicator based on a multicolor image pattern. The scale bar is 2 mm. e) Smartphone-based sensing system for both quantitative estimation and multianalyte identification. The app automatically matches the photograph of samples with the closest records in the database and gives the result of detection. Quantitative sensing of ethanol vapor is demonstrated as an example.

emerge immediately when the film is exposed to moisture; once the moisture is removed, instantly the letters are hidden again. This reversible encryption and decryption process can be simply triggered by breath (Movie S2, Supporting Information), providing potential for rapid information acquisition and protection in emergency, without any additional equipment (e.g., UV light source for commonly used data encryption devices[44]).

The color contrast of the decrypted image and nonimage area is caused by the thickness difference of the hydrogel films, which is proven after removing unreacted monomers. As shown in Figure 4c, a water droplet pattern is achieved after washing the hydrogel interferometer which is fabricated by spatially controlled polymerization. Treated with longer UV exposure time, the hydrogel of the image area (water droplet pattern) is thicker than that of the nonimage area (214 vs 193 nm at ambient relative humidity (RH) of 45%). With the increase of RH, the image and nonimage areas simultaneously swell and show shift within their reflection spectra (Figure S13, Supporting Information), exhibiting swelling ratios of 83.6% and 83.4%, respectively, at RH of 93% compared to the ambient RH of 45%. As a result, the colors of the pattern change along with the humidity. At relatively high RH, the increased chemical potential of surrounding water vapor boosts the swelling ratio of the hydrogel film, resulting in a significant color change even for a small alteration of humidity (e.g., as large as ≈100 nm redshift of the reflection valley from RH of 80% to 85%). Such high sensitivity induced by superlinear humidity responsiveness can be further tuned by adjusting the crosslinking density of the hydrogel (Figure S14, Supporting Information). The experimentally measured swelling ratio is consistent with the simulation result based on the theory of hydrogel swelling (Figure S19, Supporting Information). In addition to the monocolor image pattern, multicolor image patterns, such as a half–half star shown in Figure 4d, can be achieved via the same fabrication

strategy. Hence, the current adaptive platform can serve as an optical humidity indicator, with fast response (Figure S15 and Movie S3, Supporting Information). These examples demonstrate the potential of intuitive recognition with naked eye as well as accurate measurement by simply incorporating additional color (thickness) areas through on-demand patterning.

To realize portable and commercialized detection, we developed a colorimetric analysis application (app) for smartphones. As shown in Figure 4e, two functions are available in the app: measuring the concentration of a single analyte, and differentiating multiple analytes. When the photograph of an unknown sample is taken and analyzed, the app will automatically match the new image with the closest records in the database and give the result of detection (Movies S4 and S5, Supporting Information). The sensing system can be further developed for analysis of more compounds, depending on the design of adaptive sensors for the desired analytes. Through the mobile app, real-time monitoring of environment or bodily condition can be conveniently carried out.

In summary, inspired by the color change depending on the cell or protein soft layer of living organisms, we have demonstrated a hydrogel interferometer as an adaptive color platform, based on a thin hydrogel film covalently bonded on a substrate. The simple design avoids the use of photonic structure template or the careful assemblies of micro-/nanobuilding blocks to achieve adaptive coloration, providing a facilely tunable way for achieving broader functionalities. Small environmental alteration causes hydrogel thickness change and thus its interference color change. Hence, interference colors serve as a powerful tool to make very small measurements and reveal rich environmental metrics. We have also established a computational model to systematically investigate the response dynamics, which shows good theory–experiment agreement. This elucidates the mechanism and design principle for the

broad functionality. With the simple and covalently bonded structure, the hydrogel interferometer is robust, low cost, and applicable for various hydrogels. Specifically, by employing poly(HEMA-*co*-AAc) hydrogel, the interferometer can be used as a volatile-vapor sensor for high-accuracy quantitative detection, with fast response and recovery (140 and 210 ms, respectively). By integrating multiple such interferometers with different thicknesses into an array, the adaptive platform is able to recognize multiple VOCs, providing an approach for multianalyte identification by a single material. Furthermore, patterning can be facilely conducted on the platform, providing the capabilities of breath-controlled information encryption and decryption, as well as multicolor humidity indicator. To benefit its commercial applications, smartphone-based colorimetric analysis is built for portable and easy-to-use sensing systems. Our strategy of constructing adaptive color system provides a simple but general way for achieving diverse functionalities. By simply changing or modifying the hydrogel layer, this hydrogel interferometer can be readily applied in multiple areas such as high-level data security and real-time environment or health monitoring.

Supporting Information

Supporting Information is available from the Wiley Online Library or from the author.

Conflict of Interest

The authors declare no conflict of interest.

[1] R. Hanlon, *Curr. Biol.* **2007**, *17*, R400.
[2] L. M. Mäthger, R. T. Hanlon, *Cell Tissue Res.* **2007**, *329*, 179.
[3] R. M. Kramer, W. J. Crookes-Goodson, R. R. Naik, *Nat. Mater.* **2007**, *6*, 533.
[4] L. Phan, W. G. Walkup, D. D. Ordinario, E. Karshalev, J.-M. Jocson, A. M. Burke, A. A. Gorodetsky, *Adv. Mater.* **2013**, *25*, 5621.
[5] F. Liu, B. Q. Dong, X. H. Liu, Y. M. Zheng, J. Zi, *Opt. Express* **2009**, *17*, 16183.
[6] H.-B. Seo, S.-Y. Lee, *Sci. Rep.* **2017**, *7*, 44927.
[7] X. He, M. Aizenberg, O. Kuksenok, L. D. Zarzar, A. Shastri, A. C. Balazs, J. Aizenberg, *Nature* **2012**, *487*, 214.
[8] A. Shastri, L. M. McGregor, Y. Liu, V. Harris, H. Nan, M. Mujica, Y. Vasquez, A. Bhattacharya, Y. Ma, M. Aizenberg, O. Kuksenok, A. C. Balazs, J. Aizenberg, X. He, *Nat. Chem.* **2015**, *7*, 447.
[9] D. Buenger, F. Topuz, J. Groll, *Prog. Polym. Sci.* **2012**, *37*, 1678.
[10] A. Doring, W. Birnbaum, D. Kuckling, *Chem. Soc. Rev.* **2013**, *42*, 7391.
[11] R. Tamate, T. Ueki, R. Yoshida, *Adv. Mater.* **2015**, *27*, 837.
[12] Y. Liu, W. Shen, Q. Li, J. Shu, L. Gao, M. Ma, W. Wang, H. Cui, *Nat. Commun.* **2017**, *8*, 1003.
[13] T. Masuda, N. Shimada, T. Sasaki, A. Maruyama, A. M. Akimoto, R. Yoshida, *Angew. Chem., Int. Ed.* **2017**, *56*, 9459.
[14] W. Li, F. Gao, X. Wang, N. Zhang, M. Ma, *Angew. Chem., Int. Ed.* **2016**, *55*, 9196.
[15] B. Sun, Z. Wang, Q. He, W. Fan, S. Cai, *Soft Matter* **2017**, *13*, 6852.
[16] V. L. Alexeev, A. C. Sharma, A. V. Goponenko, S. Das, I. K. Lednev, C. S. Wilcox, D. N. Finegold, S. A. Asher, *Anal. Chem.* **2003**, *75*, 2316.
[17] Y. Kang, J. J. Walish, T. Gorishnyy, E. L. Thomas, *Nat. Mater.* **2007**, *6*, 957.
[18] E. Tian, J. Wang, Y. Zheng, Y. Song, L. Jiang, D. Zhu, *J. Mater. Chem.* **2008**, *18*, 1116.
[19] J.-T. Zhang, L. Wang, J. Luo, A. Tikhonov, N. Kornienko, S. A. Asher, *J. Am. Chem. Soc.* **2011**, *133*, 9152.
[20] L. B. Wang, J. X. Wang, Y. Huang, M. J. Liu, M. X. Kuang, Y. F. Li, L. Jiang, Y. L. Song, *J. Mater. Chem.* **2012**, *22*, 21405.
[21] C. Zhang, M. D. Losego, P. V. Braun, *Chem. Mater.* **2013**, *25*, 3239.
[22] C. Zhang, G. G. Cano, P. V. Braun, *Adv. Mater.* **2014**, *26*, 5678.
[23] B. Ye, H. Ding, Y. Cheng, H. Gu, Y. Zhao, Z. Xie, Z. Gu, *Adv. Mater.* **2014**, *26*, 3270.
[24] Z. Cai, D. H. Kwak, D. Punihaole, Z. Hong, S. S. Velankar, X. Liu, S. A. Asher, *Angew. Chem., Int. Ed.* **2015**, *54*, 13036.
[25] Y. Zhang, Q. Fu, J. Ge, *Nat. Commun.* **2015**, *6*, 7510.
[26] R. Pernice, G. Adamo, S. Stivala, A. Parisi, A. C. Busacca, D. Spigolon, M. A. Sabatino, L. D'Acquisto, C. Dispenza, *Opt. Mater. Express* **2013**, *3*, 1820.
[27] Y.-L. Ko, H.-P. Tsai, K.-Y. Lin, Y.-C. Chen, H. Yang, *J. Colloid Interface Sci.* **2017**, *487*, 360.
[28] J. Liu, Y. Zhang, R. Zhou, L. Gao, *J. Mater. Chem. C* **2017**, *5*, 6071.
[29] S. Lin, H. Yuk, T. Zhang, G. A. Parada, H. Koo, C. Yu, X. Zhao, *Adv. Mater.* **2016**, *28*, 4497.
[30] L. He, M. Janner, Q. Lu, M. Wang, H. Ma, Y. Yin, *Adv. Mater.* **2015**, *27*, 86.
[31] J.-W. Oh, W.-J. Chung, K. Heo, H.-E. Jin, B. Y. Lee, E. Wang, C. Zueger, W. Wong, J. Meyer, C. Kim, S.-Y. Lee, W.-G. Kim, M. Zemla, M. Auer, A. Hexemer, S.-W. Lee, *Nat. Commun.* **2014**, *5*, 3043.
[32] L. Bai, Z. Xie, W. Wang, C. Yuan, Y. Zhao, Z. Mu, Q. Zhong, Z. Gu, *ACS Nano* **2014**, *8*, 11094.
[33] T. Çaykara, C. Özyürek, Ö. Kantoğlu, O. Güven, *J. Polym. Sci., Part B: Polym. Phys.* **2002**, *40*, 1995.
[34] N. L. Smith, Z. Hong, S. A. Asher, *Analyst* **2014**, *139*, 6379.
[35] W. Hong, Z. S. Liu, Z. G. Suo, *Int. J. Solids Struct.* **2009**, *46*, 3282.
[36] S. A. Chester, L. Anand, *J. Mech. Phys. Solids* **2011**, *59*, 1978.
[37] X. Xu, A. V. Goponenko, S. A. Asher, *J. Am. Chem. Soc.* **2008**, *130*, 3113.
[38] A. Ranft, F. Niekiel, I. Pavlichenko, N. Stock, B. V. Lotsch, *Chem. Mater.* **2015**, *27*, 1961.

[39] J. H. Lee, B. Fan, T. D. Samdin, D. A. Monteiro, M. S. Desai, O. Scheideler, H.-E. Jin, S. Kim, S.-W. Lee, *ACS Nano* **2017**, *11*, 3632.

[40] Y. Huang, F. Y. Li, M. Qin, L. Jiang, Y. L. Song, *Angew. Chem., Int. Ed.* **2013**, *52*, 7296.

[41] Y. Liu, T. Minami, R. Nishiyabu, Z. Wang, P. Anzenbacher, *J. Am. Chem. Soc.* **2013**, *135*, 7705.

[42] M. Qin, F. Y. Li, Y. Huang, W. Ran, D. Han, Y. L. Song, *Anal. Chem.* **2015**, *87*, 837.

[43] M. Qin, Y. Huang, Y. N. Li, M. Su, B. D. Chen, H. Sun, P. Y. Yong, C. Q. Ye, F. Y. Li, Y. L. Song, *Angew. Chem., Int. Ed.* **2016**, *55*, 6911.

[44] X. Li, Y. Xie, B. Song, H.-L. Zhang, H. Chen, H. Cai, W. Liu, Y. Tang, *Angew. Chem., Int. Ed.* **2017**, *56*, 2689.